Studying Remediation Processes Using a Dimensionless Classification of Potential Storage Sites

Dan Bossie-Codreanu

Available online at www.sciencedirect.com

ScienceDirect

Energy Procedia 114 (2017) 5500 – 5520

Energy Procedia

13th International Conference on Greenhouse Gas Control Technologies, GHGT-13, 14-18 November 2016, Lausanne, Switzerland

Studying Remediation Processes using a Dimensionless Classification of potential storage sites

Dan Bossie-Codreanu

IFPEN, 1 et 4 Av. Bois-Préau, 92852 Rueil-Malmaison, France

Abstract

The current CO_2 storage operation requires a thorough integrated qualification process consisting in storage evaluation, leakage risk analysis and remediation planning in case of leaking. One of the current methods considered as a remediation method is the re-production of the CO_2. This paper presents results of a "generic" qualification of storage remediation capacity, based on a methodology using a dimensionless analysis of the potential aquifer sites supposed to qualify for storage.

The methodology consists in building a data-base of dimensionless numbers governing the storage, leading to an experimental design based on the minimum/maximum values found within the data-base. Further reduction of the cases under study was achieved through a fractional experimental method, consisting in balancing the experiments, therefore achieving a workable statistical representative number of cases. Parameters difficult to obtain from the field were generated from literature and re-production of CO_2 simulations were performed on all cases, representing the full variability of dimensionless numbers encountered in the field. The re-production was initiated after an injection period. Results were analyzed in terms of the net ratio of CO_2 produced/CO_2 injected leading to the concept of "remediation" efficiency, attached to any site to which the similar dimensionless numbers are associated. In that sense the approach is considered as being generic. The qualitative behavior of the CO_2 plume and the over-pressure criteria governing the safety of the storage are also discussed.

Peer-review under responsibility of the organizing committee of GHGT-13.

Keywords: CO2 Storage;Remediation;Qualification;Methodology

Peer-review under responsibility of the organizing committee of GHGT-13.
doi:10.1016/j.egypro.2017.03.1692

1. Introduction

The remediation method considered in this study consists in producing the CO_2 from the storage site. In principle, a remediation method in case of a leak would be to produce somehow the CO_2 from the "plume" zone. Many methods study such situations, recommending injection or production schemes within the "leaking" plume. As attractive as it may appear, this solution type doesn't seem very practical. On one hand, it implies that the leaking locations are more or less well identified, and therefore where the highest CO_2 concentration occurs. On the other hand, it also implies that our knowledge of the heterogeneity above the cap-rock is well known. This is far from being true. Furthermore, this approach will inherently cost more since it requires the drilling of an additional well within the leaking zone. Here, the term remediation implies a corrective action which aims at restoring the storage integrity, canceling the pressure differential between the storage zone and the pressure occurring above cap-rock. Therefore the method used is to produce the CO_2 directly from the from the original injection well. The production occurs at a constant rate, pursued as long as pressure in the reservoir doesn't reach its original value. This approach has the advantage to be quick in terms of implementation and less costly. The main disadvantage consists in not treating directly the leakage damage, leaving the "leaked" volume to heal itself (ex. by dilution between the point of leaking and the surface). We contend that the remediation by direct CO_2 production could be viable if monitoring methods are designed so as to allow an early warning, thus implementing quickly a direct production, and thus reducing the surface risks to a minimum.

2. Building the Problem

2.1. Theoretical Foundations

The movement of CO_2 in the groundwater aquifer during injection, potential leaking and possible remediation is complex and depends on the interplay of many factors. These factors include gravity effects, capillary forces, and viscous forces as well as the impacts from dissolution/ex-solution of the CO_2 with the water. In order to obtain a "generic" simulation framework, the following methodology followed was applied:

Step1: Dimensionless Numbers and Experimental Design Definition

- Definition of process dimensionless Numbers (DN). A series of pertinent dimensionless numbers governing injection and evolution of the CO_2 plume, using pertinent knowledge obtained by the oil industry (reservoir engineering).
- Building a data base (DB) of DN. Based on parameters making up the dimensionless numbers, an investigation of their value was collected from field cases already performed, using literature data, and a DB build accordingly.
- Using the value range of each DN, a Min/Max criteria allowed a fractional experimental design, thus reducing the number of cases.

Step2: Definition of a series of scenarios of CO_2 production. Based on the above a series of simulation covering all possible cases was build and several production scenarios were considered, stemming from a common initial CO_2 injection scheme which establishes an average original saturation field. These scenarios account for the rate production, acknowledging the possibility of water coning, which in the case of CO_2 production can be favorable, since it will favor the production of water which is probably easier to dispose.

Step3: Perform simulations on all cases defined in Step2

Step4: Analyze results and define criteria by which simulations will be evaluated in terms of safety and process performance (ex. % of CO2 recovered by comparison to CO2 injected).

Theoretically, the dimensionless numbers which can used have been identified using literature of CO_2-EOR which aimed originally at scaling the CO_2 injection Shook *et al*. [1], Rivas *et al*. [2], Diaz *et al.* [3]. Scaling consists in extrapolating results obtained at one scale size to another scale. This process produces dimensionless groups, which then serve as a basis of comparison between scales. These are combination of properties such that the dimensions of the properties composing the dimensionless group cancel each other to produce a final group with no dimensions. A process can be described by independent and dependent dimensionless variables. When the independent dimensionless groups for that group are identical, the dependent dimensionless group will also be identical. This implies that systems with completely different dimensional properties but similar dimensionless properties have a similar dimensionless response, allowing a comparison between scales. The dimensionless groups retained for the description of the injection/production CO2 process are:

Aspect Ratio (R_L): This is a measure of the communication between fluids in the horizontal direction relative to the vertical one. The aspect ratio governs the vertical equilibrium (VE), representing the state of maximum cross-flow, occurring when the forces in the transverse direction is zero. The greater the aspect ratio, the closer it is to vertical equilibrium (well approximated for aspect ratios greater than 10).

$$R_L = \frac{L}{H}\sqrt{\frac{k_z}{k_x}} \tag{1}$$

where L is the reservoir length, H is the thickness, k_z is the vertical permeability and k_x is the horizontal permeability.

Dip angle group (Nα): Long, thin, dipping reservoirs will have greater values of Nα, lessening the potential impact of gravity overriding, while thicker, shorter reservoirs (low Nα) increase the potential impact of gravity overriding.

$$N_\alpha = \frac{L}{H}\tan\ \alpha \tag{2}$$

where α is the reservoir angle with the horizontal

Mobility Ratio (M): Mobility relates the ability of gas and water to move relative to each other and are used to evaluate sweep efficiencies.

$$M_g^w = \frac{k_{rg}^o \mu_w}{k_{rw}^o \mu_g} \tag{3}$$

where μ_g and μ_w are gas and water viscosity and Kr_g° and Kr_w° are relative permeability end-points for gas and water

Buoyancy Number (Ng): The buoyancy number is the ratio of the gravity forces resulting of the density difference to the viscous forces in a reservoir. Larger values of Ng indicate larger density differences between fluids and therefore a higher potential for segregation. Thus, the Ng value governs the shape of the CO2 from its injection point (lower Ng values favoring a more cylindrical shape).

$$N_g = \frac{H\Delta\rho g\ \cos\ \alpha}{\Delta P} \tag{4}$$

where Δρ is the density between gas sand water, g is the gravity constant and ΔP is the difference in pressure between the injection and the reservoir.

Capillary Number (NPc): The capillary number is the ratio of the viscous forces to the capillary ones. It governs the amount of trapping which may occur in an aquifer storage. Capillary forces increase with capillary pressure.

$$N_{Pc} = \frac{\Delta P}{\sigma}\sqrt{\frac{k}{\phi}} \tag{5}$$

where σ is the interfacial tension and φ is the porosity.

Heterogeneity (VDP) – Dykstra-Parsons method: This method is simple, allowing the generation of a vertical (and possibly horizontal) permeability heterogeneity. It is expressed as a variance of the permeability where K_x is the permeability with a probability of x %. The index is expressed by:

$$VDP = \frac{K_{50} - K_{84.1}}{K_{50}} \tag{6}$$

The significance of such a definition can be seen in Figure 1.

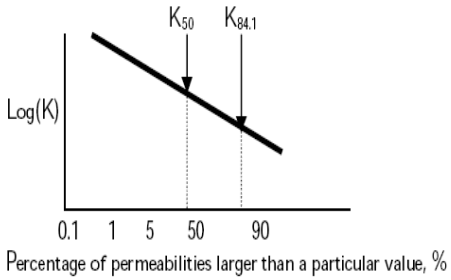

Figure 1. Illustration of the VDP concept

A completely homogeneous system has a VDP = 0 and a completely heterogeneous system has a VDP = 1. Heterogeneity is viewed as a layered system to which a permeability is assigned per layer. Thus, the method used in this study consists in assuming some VDP value (from statistics issued from hydrocarbon reservoirs), and then assign a permeability to each layer, inverting the VDP function. Vertical permeability is calculated from the horizontal value (ex. $K_z = 0.1\ K_x$). Porosity is assigned from the K-PHI relationship corresponding to the field under study, often available.

The question may be raised on why geostatistical methods are not used here. The answer is simple. Geostatistical data such as correlation lengths obtained from variogram analysis imply the existence of many wells so as to determine the existence of such correlations lengths. Furthermore, if correlative relations could be found at the facies "level", such as porosity which can be correlated for particular deposition environments it is hardy the case for permeability (outcrop studies have proven that). Using petrophysical properties for characterization would need the development of flow-units, which is not easy to Data base of geostatistical parameters for aquifers or hydrocarbon reservoirs are not easy to come by. By opposition, VDP statistics for many reservoirs have been collected (Hirasaki *et al* [4], Jensen *et al.* [5], Dykstra *et al.* [6]) and thus we can use these for our modeling purpose. While recognized as being imperfect, this method accounting for heterogeneity, given its simplicity, is considered as adequate for this study.

In our case, two representative values of VDP were considered - VDP = 0.6 and 0.8 as seen in Figure 2 below (Hirasaki *et al* [5].

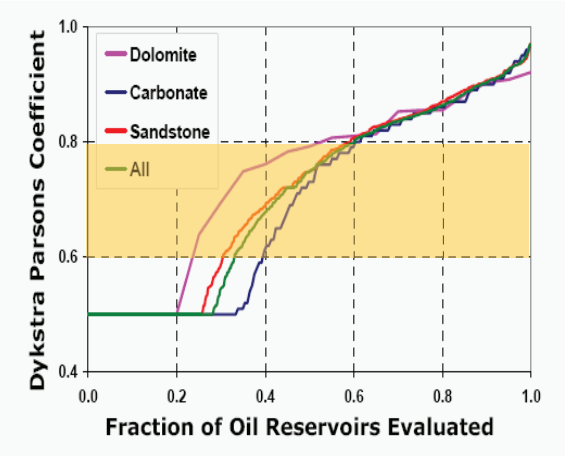

Figure 2. VDP value depending on the reservoir type

Injection pressure (P_i): This ratio determines the dimensionless injection pressure with regard to the fracturing pressure, considered as a limiting pressure for CO2 operations. For all simulations cases two scenarios were chosen, based on over-pressure data obtained from traditional CH4 storage operations.

$$P_i = \frac{P_{inj}}{P_{fract}} \tag{7}$$

Residual gas saturation (S_{gr}): Residual gas saturation controls the volume of gas trapped in that portion of the reservoir that has experienced water encroachment. As water moves into a rock volume filled with gas, the water displacement of the gas is incomplete. The water fills pores and pore throats, causing capillary pressure and relative permeability effects to stop the flow of gas and allow only water to pass through the rock volume. This results in gas being trapped behind the encroaching waterfront as residual gas. The volume and location of the residual gas are controlled by the distribution of the petrophysical properties. The trapping characteristics used were calculated from the relation of Holtz [22].

2.2 Data Base Building

The data-base of dimensionless numbers was built from information obtained from different publications describing field injections (Bachu *et al*. [7]., Bachu S. [8], Flett *et al*. [9], Hosa *et al*. [10]). The total number of sites qualifying for the data base is 60, of which 40 are aquifers and 20 reservoirs.

The theoretical analysis identified eight dimensionless groups characterizing the CO_2 storage. Further analysis of the available data lead to a reduction of the groups considered. Thus, only five groups were retained to represent the variability of all cases, namely the Aspect Ratio (R_L), the Dip angle group (N_α), the Mobility Ratio (M), the Buoyancy Number (N_g) and the Capillary Number (N_{Pc}). The other groups, namely the Residual gas saturation, VDP and Injection Pressure are estimated, making up the different simulation group scenarios. Results from the Data-Base are shown below in Figure 3 through 8.

Aspect ratio

Min = 1.58

Max = 6.32

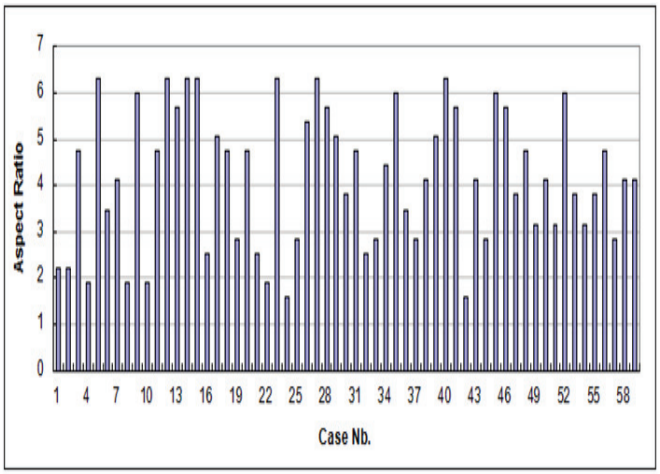

Figure 3. Aspect Ratio obtained for all investigated cases

As seen, no value among all cases considered reaches a value of 10, which is theoretically a value approximating a perfect vertical equilibrium.

Dip Number

Min = 0.17

Max = 3.52

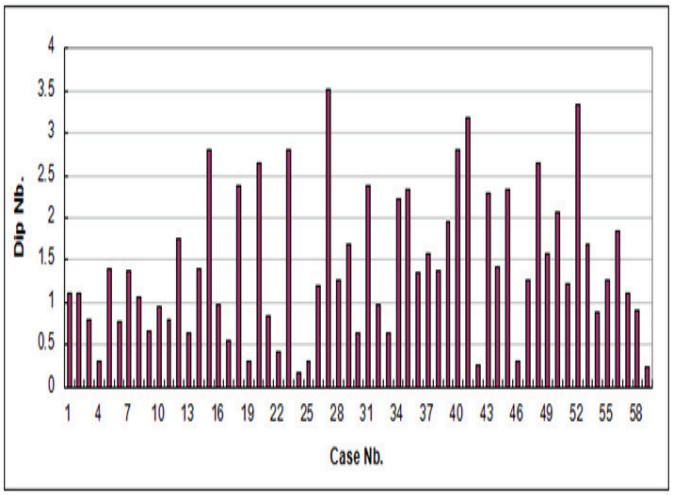

Figure 4. Aspect Ratio distribution obtained for all investigated cases

Long, thin dipping reservoirs have greater Dip Angle numbers, lessening the potential impact of gravity overriding. It also has an impact on the shape of the interface between displaced and displacing fluids. The lower the value of the number the more the interface parallel to the fluid movement. By opposition, the higher the value, the is most perpendicular to the fluid movement. In developing the statistic angle values varying between 1 and 10 degrees were used.

Mobility Ratio

Min = 1.44

Max = 54.06

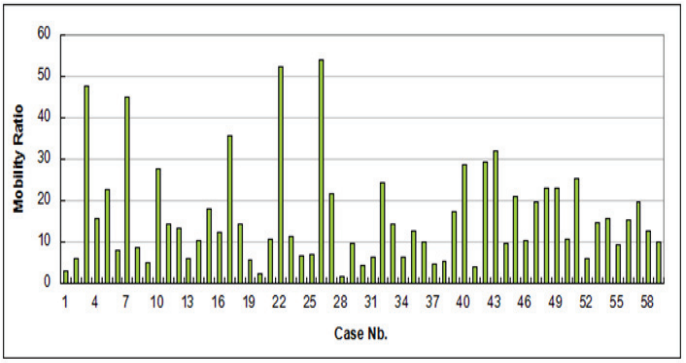

Figure 5. Mobility Ratio distribution obtained for all investigated cases

This is the ratio of the viscous forces of one fluid relative to the other. In theory the closest the ratio is to 1.0 the more stable the recovery of CO_2 will be. High values such as the ones recorded here using our data base of aquifer projects shows values up to 54.0 (for oil reservoirs it can go up to 45.0), indicative of conditions where displacement will be highly unfavorable.

Buoyancy Number

Min = 13.89

Max = 1562.1

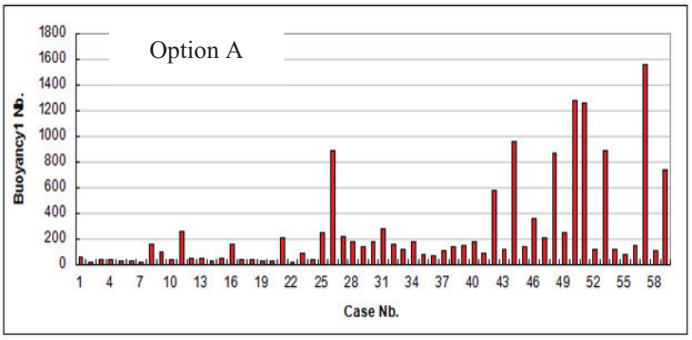

Min = 1.73

Max = 195.26

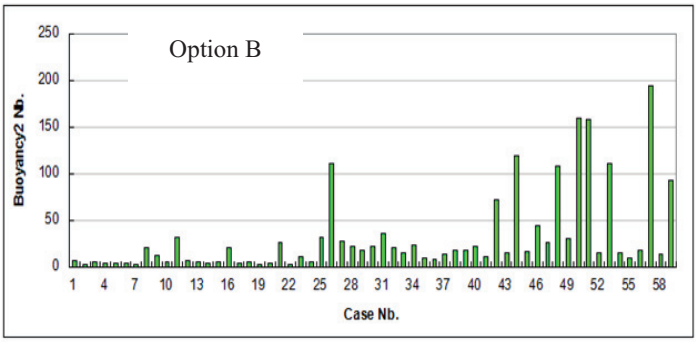

Figure 6. Buoyancy Number distribution obtained for all investigated cases (Option A -Top and B - Bottom)

The buoyancy group requires a ΔP term between the injection pressure and the reservoir pressure. The injection pressure is related to the fracturing pressure which represents a potential risk when storing the CO_2 - the risk not being necessarily the fracture itself, but the potential impact it could create on the well completion (cementation), thus creating a potential leaking path. Thus, two hypothesis are made. The first one assumes that $P_{inj} = 1.1P_{res}$ (option a) while the second one is that $P_{inj} = 1.8P_{res}$ (option b). Results are shown below. Given the fact that the only values changing between the two options are the injection pressure, the variability among values stays the same.

Capillary Number

The capillary group variability is shown below (Figure 7).

Min = 1.4E-04

Max = 3E-03

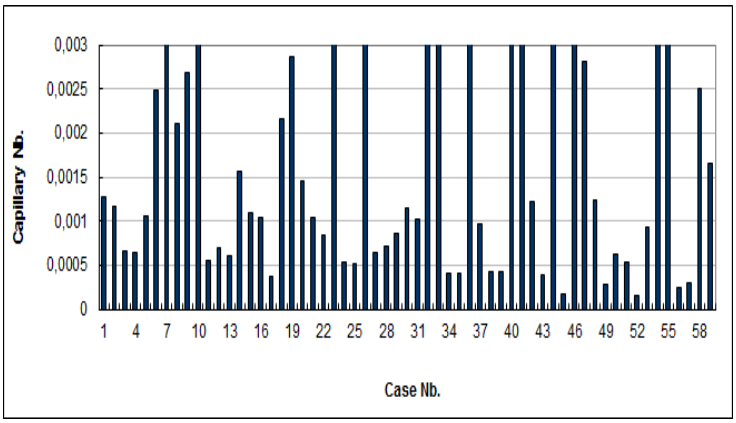

Figure 7. Capillary Number distribution obtained for all investigated cases

Like the other constitutive relationships describing multiphase flow, capillary pressure and relative permeability, the IR characteristic of a rock is considered to be invariant across a wide range of fluid pairs and conditions of temperature, pressure and brine salinity so long as the wetting state of the system remains similar between systems.

It is well known that these properties will vary, however, and if these conditions control the wetting state of the system (Salathiel [11]) or the flow velocity v, viscosity μ and interfacial tension σ combine in a way such that the dimensionless capillary number, $Nc = v\mu/\sigma$, exceeds a critical value for desaturation. For Berea sandstone, for example, this has been observed to be in the range $Nc > 10^{-5} - 10^{-4}$ (Taber [12]). For natural rocks representative of a wide variety of pore structures the range of capillary numbers for desaturation extends to $Nc > 10^{-7} - 10^{-4}$ (Lake et al., [13]). Observations of the wetting state of the CO2 brine system have raised doubts about whether these general observations extend to CO2 displacement. Contact angle, conventionally measured in the wetting phase, water, was observed to increase (weakening water wetting) with pressure in work of Broseta *et al*. [14] Chiquet *et al*. [15] or Iglauer *et al.* [16] , by opposition to the work of Espinoza *et al.* [17], Farokhpoor *et al.* [18], and Wang et al. [19]. Contact angle was observed to increase significantly with brine salinity in work by Espinoza et al. [17],, but not in Broseta *et al.* [14], Chiquet *et al.* [15]. The work of Farokhpoor *et al.* [18], Saraji *et al.* [20] investigated the dependency of contact angle on temperature but a clear trend was not observed. A recent review of the subject (Iglauer *et al* [21].) highlights the challenging nature of these experiments and summarizes that the wide range of behavior observed can be attributed largely to differences in surface roughness and surface contamination between studies. Thus, it is difficult a-priori to estimate the role this number will play during the simulation of an injection/production process as envisioned here. We expect the residual saturation to play a larger role through the Kr trapping effects and thus indirectly reflecting the importance of capillary trapping.

The Sgr term

In addition to all the dimensionless groups chosen as representative of the CO_2 storage, the maximum gas strapping saturations are shown, in order to define a representative value range to be used with all scenarios (see Figure 8).

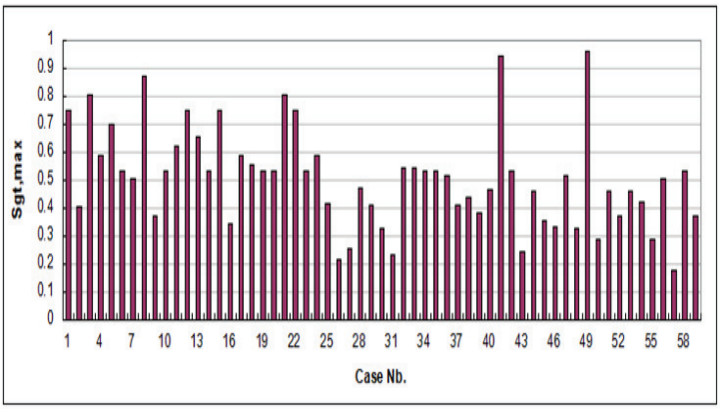

Figure 8. Sgt_{max} distribution obtained for all investigated cases

When studying the distribution of reservoirs within our data-base by Sgt_{max} class-values, we observe very high values of trapped gas saturations for reservoirs of low porosity values. These potential candidates should be excluded from potential storage sites given their porosity values which in term controls the storage capacity.

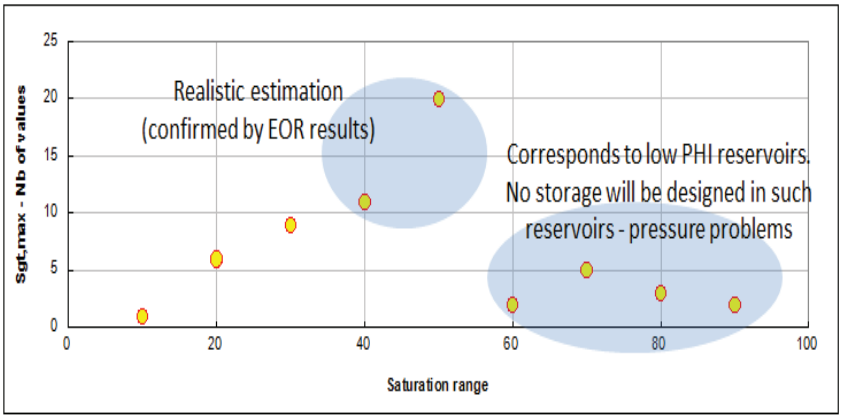

Figure 9. Reservoir distribution classified by trapped gas saturation values

The value most representative are considered as S_{gtmax} = 0.45. The EOR operations have shown from a simple material balance (amount of CO_2 injected – amount of CO_2 produced) that about 40 to 50 % of the CO_2 injected stays trapped. These figures are worth considering over eventual core-floods since they are obtained at a macroscopic scale (realistic scale).

From all the dimensionless terms defined above, considering a representative variability we are looking after, and considering the min/max values of all dimensionless groups, we designed 4 main scenarios, shown below.

Scenario 1	-1	1
VDP	0.6	
	Min	Max
Aspect Ratio	1.58	6.32
Dip	0.17	3.52
Mobility Ratio	1.44	54.06
Buoyancy1	13.89	1562.1
Capillary	0.000301	4.68

Scenario 2	-1	1
VDP	0.6	
	Min	Max
Aspect Ratio	1.58	6.32
Dip	0.17	3.52
Mobility Ratio	1.44	54.06
Buoyancy1	1.73	195.26
Capillary	0.000301	4.68

Scenario 3	-1	1
VDP	0.8	
	Min	Max
Aspect Ratio	1.58	6.32
Dip	0.17	3.52
Mobility Ratio	1.44	54.06
Buoyancy1	13.89	1562.1
Capillary	0.000301	4.68

Scenario 4	-1	1
VDP	0.8	
	Min	Max
Aspect Ratio	1.58	6.32
Dip	0.17	3.52
Mobility Ratio	1.44	54.06
Buoyancy1	1.73	195.26
Capillary	0.000301	4.68

Figure 10. All scenarios considering values of dimensionless numbers

The Scenarios above consider two VDP values (0.6 and 0.8), along with two buoyancy numbers (corresponding to two injection conditions; one leading to higher overpressures after 4 years than the other – these numbers being derived from a pressure difference formulation between reservoir pressure and injection pressure.

In summary six numbers are considered (including two different buoyancy numbers) but only five are considered for an experiment design for each VDP chosen (in our case 0.6 and 0.8)

2.3 Experimental Design & Optimization

The design of experiments (in our case simulations) is a planned approach aiming to determine cause and effect relationships, applied to any process with measurable inputs and outputs. The aim of designing experiments is to identify the factors which cause changes in the responses, and predicting them in a simple mathematical form. In our case we used a fractional factorial design to reduce the number of simulations to be run in order to obtain a representative response relationship.

Factorial design means that all possible combinations of the levels of the factors are investigated in each complete trial or replication of the experiment (simulation). One of the most widely used case of factorial design is using K factors with two levels. These two levels are denoted as (-1) for the minimum value and (+1) for the maximum one. Therefore, a 2^k factorial design requires 2^k runs to perform the analysis. For a five dimensionless group problem, considering the maximum and minimum values, the total number of simulations to perform are 32. In our case since four main scenarios are considered, 128 simulation in theory cover the entire "experiment", including all interactions. This is shown in Figure 11 in which A= Aspect Ratio, B=Dip Number, C= Mobility Ratio, D= Buoyancy Number (either 1 or 2 depending on the injection scheme chosen) and E= Capillary Number.

Results of the full experimental design are shown in Fig. 11, including the interaction terms, considering all parameters (5 parameters) or any combination (2,3 or 4 parameters) . Along with the full experimental design, the sum of all parameters is shown in the last column, helping in reducing the number of simulations.

	A	B	C	D	E	ABCDE	AB	AC	AD	AE	BC	BD	BE	CD	CE	DE	ABC	ACD	ADE	BCD	BDE	CDE	ABCD	BCDE	Sum
1	1	1	1	1	1	1	1	1	1	1	1	1	1	1	1	1	1	1	1	1	1	1	1	1	18
2	-1	1	1	1	1	-1	-1	-1	-1	-1	1	1	1	1	1	1	-1	-1	-1	1	1	1	-1	1	2
3	1	-1	1	1	1	-1	-1	1	1	1	-1	-1	-1	1	1	1	-1	1	1	-1	-1	1	-1	-1	0
4	1	1	-1	1	1	-1	1	-1	1	1	-1	1	1	-1	-1	1	-1	-1	1	-1	1	-1	-1	-1	-2
5	1	1	1	-1	1	-1	1	1	-1	1	1	-1	1	-1	1	-1	1	-1	-1	-1	-1	-1	-1	-1	-4
6	1	1	1	1	-1	-1	1	1	1	-1	1	1	-1	1	-1	-1	1	1	-1	1	-1	-1	1	-1	2
7	-1	-1	1	1	1	1	1	-1	-1	-1	-1	-1	-1	1	1	1	-1	-1	-1	-1	-1	1	1	-1	-4
8	1	-1	-1	1	1	1	-1	-1	1	1	1	-1	-1	-1	-1	1	1	-1	1	1	-1	-1	1	1	0
9	1	1	-1	-1	1	1	1	-1	-1	1	-1	-1	1	1	-1	-1	-1	1	-1	1	-1	1	1	1	0
10	1	1	1	-1	-1	1	1	1	-1	-1	1	-1	-1	-1	-1	1	1	-1	1	-1	1	1	-1	1	0
11	-1	-1	-1	1	1	-1	1	1	-1	-1	1	-1	-1	-1	-1	1	-1	1	-1	1	-1	-1	-1	1	-4
12	1	-1	-1	-1	1	-1	-1	-1	-1	1	1	1	-1	1	-1	-1	1	1	-1	-1	1	1	-1	-1	-2
13	1	1	-1	-1	-1	-1	1	-1	-1	-1	1	1	1	-1	1	1	-1	1	1	1	-1	1	-1	-1	0
14	-1	-1	-1	-1	1	1	1	1	1	-1	1	1	-1	1	-1	-1	-1	-1	1	-1	1	1	1	-1	2
15	1	-1	-1	-1	-1	1	-1	-1	-1	-1	1	1	1	1	1	1	1	1	1	-1	-1	-1	-1	1	2
16	-1	-1	-1	-1	-1	-1	1	1	1	1	1	1	1	1	1	1	-1	-1	-1	-1	-1	-1	-1	1	6
17	1	-1	-1	-1	-1	1	-1	-1	-1	-1	1	1	1	1	1	1	1	1	1	-1	-1	-1	-1	1	2
18	-1	1	-1	-1	-1	1	-1	1	1	1	-1	-1	-1	1	1	1	1	-1	-1	1	1	-1	-1	-1	0
19	-1	-1	1	-1	-1	1	1	-1	1	1	-1	1	1	-1	-1	1	1	-1	1	-1	1	-1	-1	-1	2
20	-1	-1	-1	1	-1	1	1	1	-1	1	-1	1	-1	1	-1	1	-1	1	1	1	1	1	-1	-1	4
21	-1	-1	-1	-1	1	1	1	1	1	-1	1	1	-1	1	-1	-1	-1	-1	1	-1	1	1	1	-1	2
22	1	1	-1	-1	-1	-1	1	-1	-1	-1	-1	-1	-1	1	1	1	-1	1	1	1	1	-1	1	-1	0
23	-1	1	1	-1	-1	-1	-1	-1	1	1	1	-1	-1	-1	-1	1	-1	1	-1	-1	1	1	1	1	0
24	-1	-1	1	1	-1	-1	1	-1	-1	1	-1	-1	1	1	-1	-1	1	-1	1	-1	1	-1	1	1	0
25	-1	-1	-1	1	1	-1	1	1	-1	-1	-1	-1	-1	-1	1	1	-1	1	-1	1	-1	-1	-1	1	-4
26	1	1	1	-1	-1	1	1	1	-1	-1	1	-1	-1	-1	-1	1	1	-1	1	-1	1	1	-1	1	0
27	-1	1	1	1	-1	1	-1	-1	-1	1	1	1	-1	1	-1	-1	-1	-1	1	1	-1	-1	-1	-1	-6
28	-1	-1	1	1	1	1	1	-1	-1	-1	-1	-1	1	1	1	1	-1	-1	-1	-1	1	1	1	-1	-4
29	1	1	1	1	-1	-1	1	1	1	-1	1	1	-1	1	-1	-1	1	1	-1	1	-1	-1	1	-1	2
30	-1	1	1	1	1	-1	-1	-1	-1	-1	1	1	1	1	1	1	-1	-1	-1	1	1	1	-1	1	2
31	1	-1	1	-1	1	1	-1	1	-1	1	-1	1	-1	-1	1	-1	-1	-1	-1	1	1	-1	1	1	-2
32	-1	1	-1	1	-1	-1	-1	1	-1	1	-1	1	-1	-1	1	-1	1	1	1	-1	-1	1	1	1	2
Sum	0	0	0	0	0	0																			

Figure 11. Setting up the experimental design including interactions

In order to reduce the number of simulations we can reduce use a “balance” method which adds all coefficients (1 and -1 corresponding the min and max values), including all interaction terms among all 5 dimensionless terms considered, and choose only those cases for which the sum is null. In such a way we have a balance effect of all parameters among themselves. This leads us a fractional experimental design showing 8 cases. The summary of this simple method is shown in Figure 12.

		A	B	C	D	E	ABCDE	AB	AC	AD	AE	BC	BD	BE	CD	CE	DE	ABC	ACD	ADE	BCD	BDE	CDE	ABCD	BCDE	Sum
1	3	1	-1	1	1	1	-1	-1	1	1	1	-1	-1	-1	1	1	1	-1	1	1	-1	-1	1	-1	-1	0
2	8	1	-1	-1	1	1	1	-1	-1	1	1	1	-1	-1	-1	-1	1	1	-1	1	1	-1	-1	1	1	0
3	9	1	1	-1	-1	1	1	1	-1	-1	1	-1	-1	1	1	-1	-1	-1	1	-1	1	-1	1	1	1	0
4	10	1	1	1	-1	-1	1	1	1	-1	-1	1	-1	-1	-1	-1	1	1	-1	1	-1	1	1	-1	1	0
5	13	1	1	-1	-1	-1	-1	1	-1	-1	-1	-1	-1	-1	1	1	1	-1	1	1	1	1	-1	1	-1	0
6	18	-1	1	-1	-1	-1	1	-1	1	1	1	-1	-1	-1	1	1	1	1	-1	-1	1	1	-1	-1	-1	0
7	23	-1	1	1	-1	-1	-1	-1	-1	1	1	1	-1	-1	-1	-1	1	-1	1	-1	-1	1	1	1	1	0
8	24	-1	-1	1	1	-1	-1	1	-1	-1	1	-1	-1	1	1	-1	-1	1	-1	1	-1	1	-1	1	1	0

Figure 12. Final experimental design covering all simulations per scenario

3. Simulations Set-up

In order to perform simulations one needs to define as input a geometry (grid properties), which should be refined within the storage zone. The grid shown below is common to all simulations. Below (Figure 13) we show first an X-Y view followed by a X-Z or Y-Z view of the layering chosen.

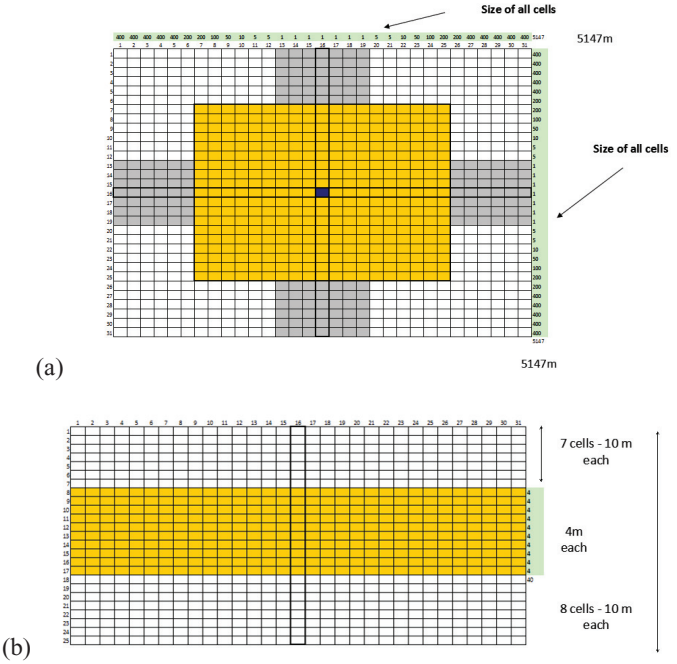

Figure 13. Grid used in X, Y and Z for all simulations: (a) X-Y and (b) X-Z or Y-Z

As seen the injection zone has been refined, in order to minimize gridding effects. The full reservoir zone is closed, considered as an injection storage zone, isolated from the rest of the field.

A petrophysical relationship between K and PHI as well as a spatial distribution of these properties has been developed using the two VDP values chosen (0.6 and 0.8), considered to cover the entire range of possible heterogeneity variation. The average permeability used is 200md and the average porosity is 0.2. Given the VDP used the minimum permeability is 43md while the maximum is 912md for VDP = 0.6 and the minimum permeability is 13md and 2874md for VDP = 0.8. Results corresponding to a stochastic draw of 8 realizations (corresponding to the 8 cases identified as representative by the experimental design) are shown below when considering an PHI range of 0.15 to 0.24, considered as representative of reservoirs in which CO_2 storage will be considered (Figure 14).

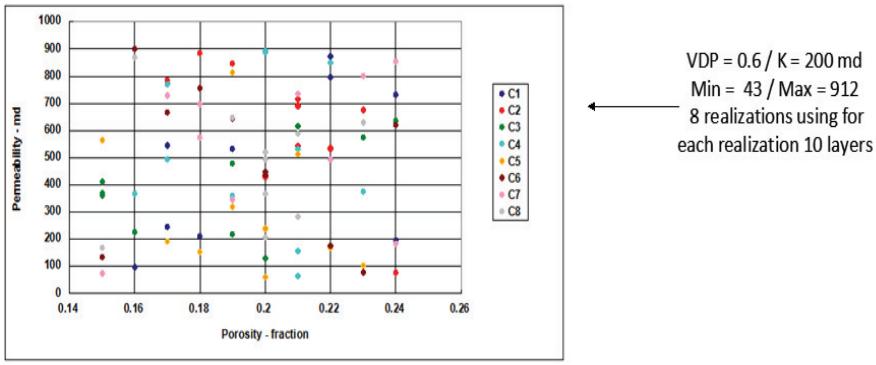

(a)

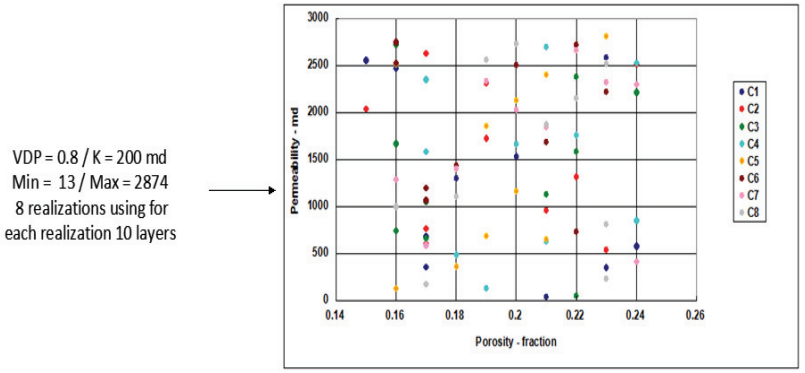

(b)

Figure 14. Permeability realizations obtained for a VDP of (a) 0.6 and (b) 0.8

These values were generated at the level of the reservoir (See grid representation above) while for the rest of the simulation domain average values were used.

The actual K vs. PHI distributions are shown below. In principle the VDP concept implies an ordering of layers within the reservoir. In our case this is not the case and all values within layers are drawn randomly within the petrophysical range values indicated. The procedure consisted to first determine a unique K-PHI relationship.within a porosity range 0.15 and 0.24 (typical of potential storage aquifers). To these porosity values are associated permeability values obtained from the VDP centered around an average permeability of 200md (again typical of what storage aquifers ought to have). The final step is to draw randomly from the porosity and permeability distribution 8 realizations which establishes 8 distributions. Results are shown in Figure 15.

For VDP = 0.6

PHI	K	PHI	K	PHI	K	PHI	K	PHI	K	PHI	K	PHI	K	PHI	K
0.24	732	0.21	691	0.15	362	0.16	367	0.22	169	0.24	620	0.21	734	0.19	646
0.24	196	0.22	534	0.15	411	0.19	361	0.2	62	0.2	448	0.24	184	0.2	521
0.22	796	0.17	784	0.23	574	0.17	769	0.21	513	0.19	645	0.24	854	0.23	630
0.17	245	0.23	676	0.2	129	0.22	850	0.19	320	0.17	667	0.18	574	0.16	868
0.18	210	0.21	715	0.24	635	0.23	374	0.15	565	0.18	756	0.18	698	0.21	283
0.17	774	0.2	428	0.15	369	0.21	64	0.17	191	0.16	901	0.22	493	0.2	495
0.16	98	0.24	76	0.21	616	0.21	531	0.18	154	0.2	437	0.23	801	0.15	169
0.22	874	0.18	884	0.16	226	0.17	495	0.19	814	0.22	175	0.15	74	0.21	589
0.19	532	0.19	847	0.19	479	0.21	156	0.2	239	0.23	78	0.17	729	0.2	368
0.17	545	0.21	543	0.19	219	0.2	890	0.23	104	0.15	134	0.19	347	0.2	206

For VDP = 0.8

PHI	K	PHI	K	PHI	K	PHI	K	PHI	K	PHI	K	PHI	K	PHI	K
0.17	354	0.17	765	0.17	1054	0.21	2697	0.2	1165	0.16	2744	0.17	588	0.17	177
0.23	2584	0.23	536	0.22	2379	0.17	1579	0.19	685	0.22	732	0.22	2657	0.18	1103
0.2	1530	0.19	2312	0.22	49	0.24	2526	0.21	651	0.17	1065	0.18	1398	0.22	2150
0.15	2554	0.22	1317	0.21	1132	0.17	2348	0.23	2806	0.18	1435	0.24	411	0.16	998
0.18	1295	0.19	1725	0.22	1583	0.21	632	0.19	1855	0.17	1197	0.2	2023	0.19	2560
0.21	37	0.15	2036	0.16	2724	0.2	1663	0.16	127	0.22	2719	0.21	1847	0.21	1870
0.24	578	0.17	607	0.24	2213	0.24	852	0.16	2517	0.23	2216	0.23	2323	0.23	811
0.16	2466	0.17	2624	0.16	1668	0.22	1757	0.21	2396	0.2	2503	0.24	2295	0.2	2732
0.17	683	0.21	958	0.16	741	0.19	127	0.2	2124	0.16	2525	0.16	1285	0.23	234
0.23	352	0.24	2514	0.17	664	0.18	487	0.18	363	0.21	1682	0.19	2330	0.23	2519

Figure 15. K-PHI distributions for all simulations

A dynamic petrophysical data set (Relative permeability Kr curves for water and CO_2). Aside from the saturation and individual curves end-points, exponents of the curves are also needed.

The first step of this data generation is to define the maximum gas saturation trapped (Sgt_{max}). Since for all realizations a different porosity distribution is used, we considered the average porosity of each realization and then using the correlation of Holtz [22] we generated the corresponding trapping gas saturation. Results are show in Figure 16.

VDP = 0.6

Sim 1	Sim2	Sim3	Sim4	Sim5	Sim6	Sim7	Sim8
0.381106893	0.363649342	0.396969158	0.378157216	0.383057333	0.384259012	0.373317673	0.381504725

VDP = 0.8

Sim 1	Sim2	Sim3	Sim4	Sim5	Sim6	Sim7	Sim8
0.384822981	0.38422881	0.386291817	0.368941326	0.38439346	0.386921737	0.367989639	0.370658978

Figure 16. Trapped CO2 saturation for all simulations using Holtz correlation

The second step is to generate the other end-point of the Kr curves, such as the Swi (for both imbibition and drainage curves since injection and imbibition have to be considered. The other factors concern the M and N Corey shape factors which have to be used. Since no clear data base is currently available in the literature we used values given by Bachu [8], concerning aquifers in Canada. We considered them as representative (Figure 17).

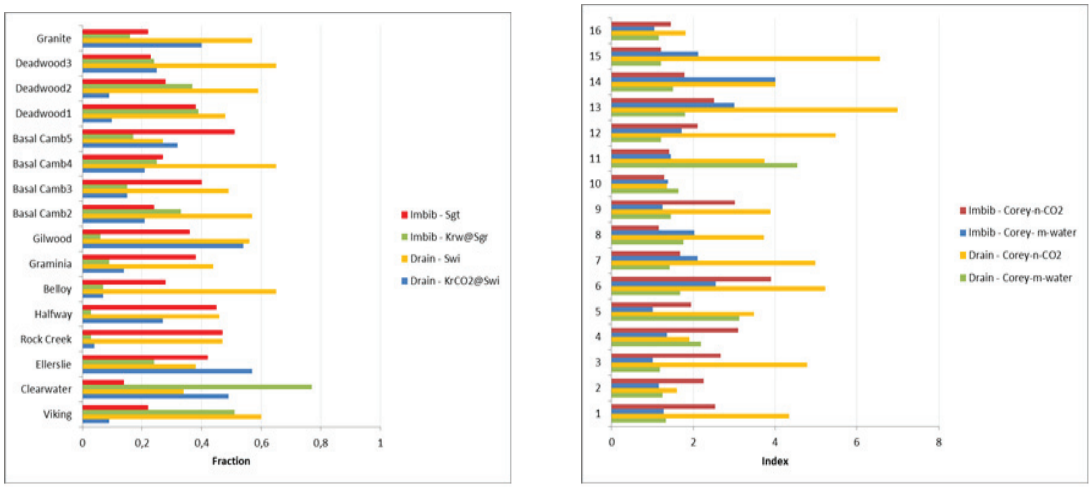

(a) (b)

Figure 17. (a) Sgt and Swi including end-points and (b) M and N Corey exponents

When summarizing all results and grouping them according to all cases simulated, for drainage and imbibition, results can be seen below (Figure 18).

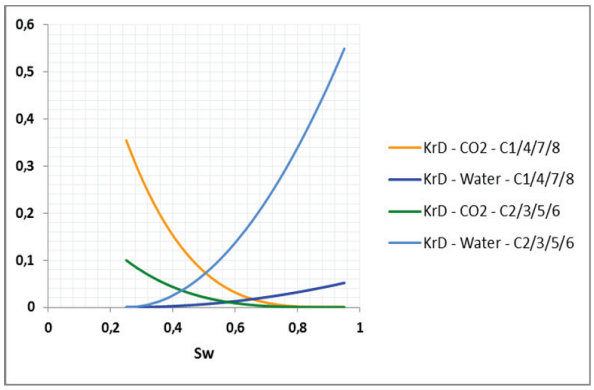

(a)

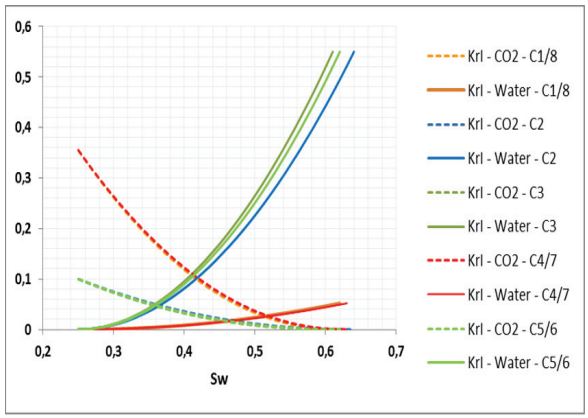

(b)

Figure 18. Kr for all cases for (a) drainage and (b) imbibition

Given all of the above we can summarize all simulation cases along two scenarios of injection corresponding to allowable overpressures: the first one corresponding to an overpressure varying between $1.1P_{res}$ and $1.2\ P_{res}$, while the other considers a variation of $1.3P_{res}$ to $1.5P_{res}$. These values are considered as typical overpressures which are seen during the storage of CH_4 which are the only reliable historical record of storage gas overpressure in our possession. This is why we considered these values for the simulations undertaken.

In summary, what has been developed are the formulation of a few dimensionless numbers characterizing the storage, the minimum and maximum values of these from a realistic data-base of reservoirs and a few simulations based on various combinations of maximum and minimum values of these dimensionless numbers. The last step is to find common values of the parameters making up these dimensionless numbers, coherent throughout and meeting the requirements of the min. and max. values. This step was done through an iterative, trial-and error process, leading to a data set of values which fit the best all dimensionless values.

Results are given in the next figures (Figure 19), for both injection schemes, leading to different overpressures expected during the various simulations undertaken.

Summary	Scenario 1 (Plim from 1.1Pres to 1.23Pres)							
	1	2	3	4	5	6	7	8
L	800	800	800	800	800	800	800	800
H	40	40	40	40	40	40	40	40
Kx	200	200	200	200	200	200	200	200
Kz	20	20	20	20	20	1,25	1,25	1,25
alpha	5	5	5	5	5	5	5	5
Krw*	0,052	0,55	0,55	0,052	0,55	0,55	0,052	0,052
KrCO2*	0,355	0,1	0,1	0,355	0,1	0,1	0,355	0,355
Muw	0,8	0,8	0,8	0,8	0,8	0,8	0,8	0,8
MuCO2	0,1	0,1	0,1	0,1	0,1	0,1	0,1	0,1
rhow	1200	1200	1200	1200	1200	1200	1200	1200
rhoCO2	500	500	500	500	500	500	500	500
Pres	14000	14000	14000	14000	14000	14000	14000	14000
Pinj	15400	15400	15400	25200	25200	25200	25200	15400
PHI	0,25	0,25	0,25	0,25	0,25	0,25	0,25	0,25
sigma	40	40	40	40	40	40	40	40

(a)

Summary	Scenario 2 (Plim from 1.3Pres to 1.5Pres)							
	1	2	3	4	5	6	7	8
L	800	800	800	800	800	800	800	800
H	40	40	40	40	40	40	40	40
Kx	200	200	200	200	200	200	200	200
Kz	20	20	20	20	20	1.25	1.25	1.25
alpha	5	5	5	5	5	5	5	5
Krw*	0.052	0.55	0.55	0.052	0.55	0.55	0.052	0.052
KrCO2*	0.355	0.1	0.1	0.355	0.1	0.1	0.355	0.355
Muw	0.8	0.8	0.8	0.8	0.8	0.8	0.8	0.8
MuCO2	0.1	0.1	0.1	0.1	0.1	0.1	0.1	0.1
rhow	1200	1200	1200	1200	1200	1200	1200	1200
rhoCO2	500	500	500	500	500	500	500	500
Pres	14000	14000	14000	14000	14000	14000	14000	14000
Pinj	16800	16800	16800	33000	33000	33000	33000	16800
PHI	0.25	0.25	0.25	0.25	0.25	0.25	0.25	0.25
sigma	40	40	40	40	40	40	40	40

(b)

Figure 19. All cases for the two injection scenarios (a) Pinj = 1.1/1.2Pres and (b) Pinj = 1.3/1.5Pinj)

An initial temperature and pressure: the initial temperature was set at 54°C (ad-hoc) whereas the initial pressure is taken as 140bars, in the middle of the perforated interval.

An injection rate corresponding to the CO_2 placement stage - injection stage: the injection rate chosen is 1M tons CO_2/year. This value is often used as a "standard" in CO_2 injection scenarios. The injection is supposed to occur over the entire reservoir height. The reservoir height considered are supposed to be realistic. Injection is set to occur for 4 years.

A production rate corresponding to the remediation stage - CO_2 production stage: the production rate was set in such a way as to reduce to the maximum the original overpressure so as recover the original reservoir pressure within 4 years. When the overpressure reaches close to zero during the production period, a balance is performed between the injected and produced CO_2 and the recovery factor is calculated.

The total number of simulations is 32 considering the experimental design performed, the VDP (heterogeneity) and the two injection scenarios.

4. RESULTS and DISCUSSION

The fraction of the CO_2 produced can be considered as the % of CO_2 recovered. Results show (Figure 20) the following, considering simulated scenarios simulated, along with the highest (yellow) and the lowest (blue) recovery factor depending on the injection scenario.

Scenario1			Scenario2		
Case	CO2-Recovery	Over-Pressure	Case	CO2-Recovery	Over-Pressure
1	0.254	1.16	1	0.306	1.47
2	0.21	1.13	2	0.445	1.47
3	0.24	1.17	3	0.45	1.45
4	0.26	1.23	4	0.31	1.49
5	0.24	1.19	5	0.41	1.42
6	0.43	1.2	6	0.56	1.5
7	0.3	1.16	7	0.33	1.47
8	0.28	1.19	8	0.332	1.49
9	0.18	1.14	9	0.256	1.42
10	0.1	1.12	10	0.316	1.436
11	0.13	1.15	11	0.315	1.468
12	0.2	1.13	12	0.286	1.438
13	0.11	1.16	13	0.248	1.345
14	0.2	1.16	14	0.381	1.427
15	0.25	1.14	15	0.333	1.408
16	0.29	1.16	16	0.34	1.422

Figure 20. Overall results for all simulated cases

Among all simulated cases, Case 6 shows the highest recovery for both scenarios whereas the lowest are Case 10 for Scenario 1 and Case 13 for Sceanrio2. The highest recoveries occur for more homogeneous cases whereas the lowest occur for cases which are the most heterogeneous. Overall results are shown in Figure 21.

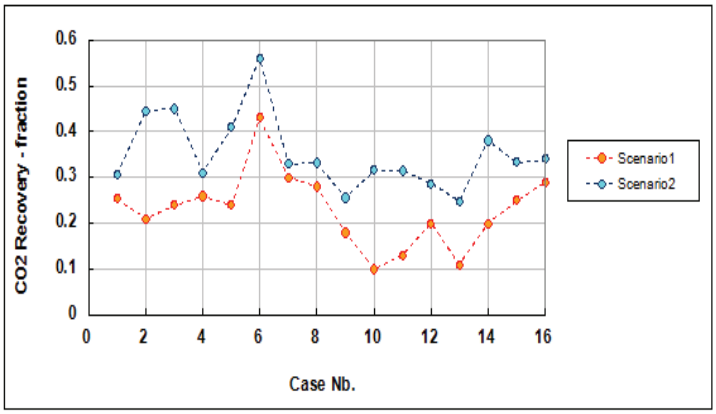

Figure 21. CO2 recovery factors

Recoveries are higher for scenario 2 corresponding to higher initial injection rates. These recoveries are in line with examples from the industry corresponding to recoveries of CO_2 during EOR operations in the Permian Basin (Hadlow [22]). Since initially a greater quantity of CO_2 was injected it is normal to record higher rates of CO_2. The main phenomena is the CO_2 confinement within the reservoir and the assurance that during the injection the gravity override does not cause a CO_2 accumulation at the top of the injection formation, below the cap-rock. This is

precisely why the injection section was set at some distance from that layer, in order to study such an override. If the injection section is set right below the cap-rock, while recoveries of the CO_2 will not be under gravity override influence, the risk concerns only the integrity of the cap-rock, whereas if the injection is performed lower, away from the cap-rock risk, the CO_2 recovery will be influenced by the override. Estimating aquifer properties which favors the CO_2 confinement within a dedicated reservoir zone is easier to do than an overall integrity assessment of the cap-rock. This is also a reason why injection was set in a zone away from the cap-rock.

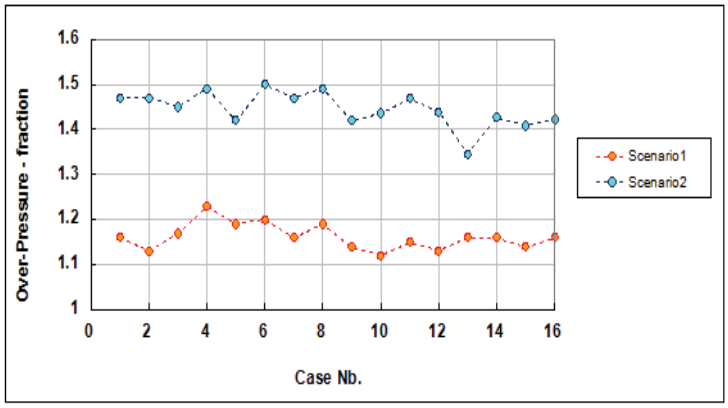

Figure 22. Over-Pressure – fraction of the Pres.original

Maximum over-pressure results for all cases are rather homogeneous throughout all simulations performed (Figure 22). The over-pressure variability is caused by the variation of porosity created by the different realizations. Of course, injection scenario 2 corresponding to higher injection pressures creates higher over-pressures.

If we consider the reservoir characteristics collected and used above as being representative of aquifers which could be candidates for CO_2 storage, results of all the simulations can be used to develop multiple regression relations which give the CO_2 recovery factors as functions of dimensionless numbers. These are:

- For Injection Scenario 1

$$\%CO_2 \text{ Rec.} = - 0.0128 - 0.0195 (A.Ratio) - 0.0073 (Dip) + 0.00048 (M) - 0.000036 (Ng) + 0.0052 (Ca) + 1.81 Sgr - 0.47 (VDP)$$

- For Injection Scenario 2

$$\%CO_2 \text{ Rec.} = 0.958 - 0.0184 (A.Ratio) - 0.0016(M) - 0.000089 (Ng) + 0.0068 (Ca) - 0.502 Sgr - 0.41 (VDP)$$

These relations show that CO_2 recoveries depend essentially on the amount of trapping occurring in-situ as well as the heterogeneity of the system. If all dimensionless elements can be estimated for a prospect, the above relations could be used to select storage sites (or rank them) according to the amount of CO_2 which could be recovered. Yet, these relationships do not reflect enough the importance of the gravity override occurring due to vertical permeability or density difference between water and CO_2 causing the CO_2 to move in upper layers.

If we consider Scenario 1, the lowest recovery occurs for Case 10. The saturation situation can be seen in the Figure 23 below. After 4 years of injection most saturation accumulation occurs below the cap-rock. Given the fact that production is designed to occur within the injection interval (realistic design), the final recovery due to re-production "pushes" most of the CO_2 in the upper layers causing the initial reservoir to be depleted, leaving most of the CO_2 in the upper layers.

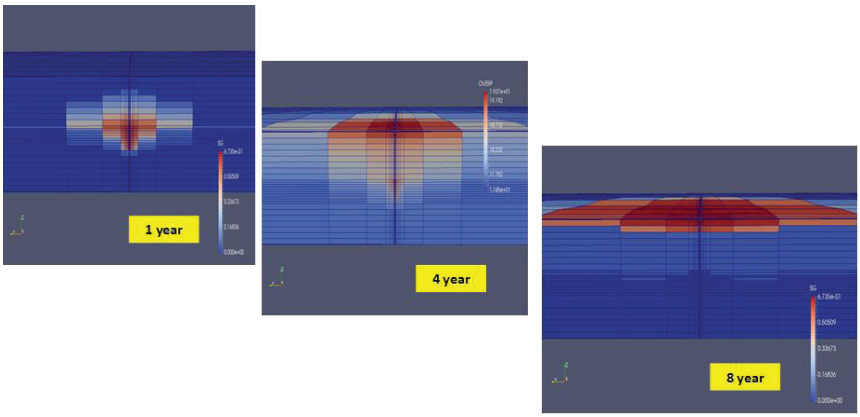

Figure 23. Scenario 1 (Case 10) - Sg evolution throughout the injection - production process

If now we compare for the same injection scenario, Case 10 corresponding to the lowest recovery to Case 6, corresponding to the highest recovery, we observe that CO_2 throughout the injection (after 4 years) is confined within the original reservoir (Figure 24). Therefore, during the production step, most of the CO_2 is able to be produced, thus achieving high recovery rates, only ruled by the Kr curves and the trapping characteristics.

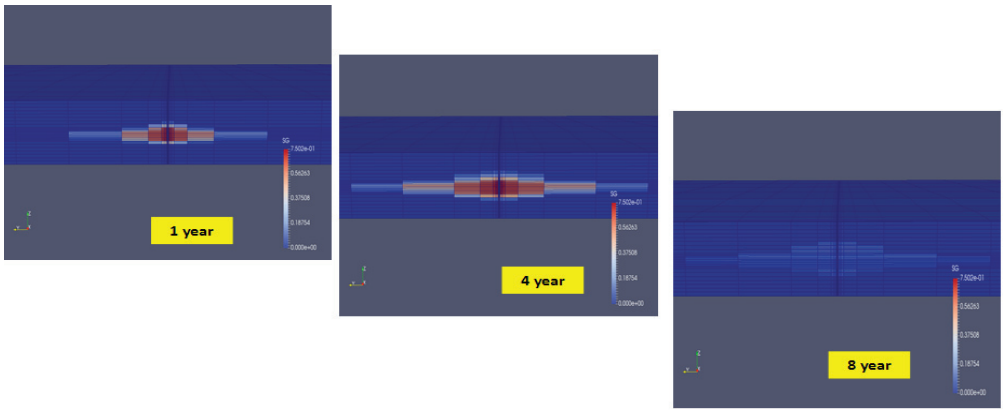

Figure 24. Scenario 1 (Case6) - Sg evolution throughout the injection - production process

When comparing the dimensionless numbers governing these extreme cases we observe the following (Figure 25)

Case	CO2 Recovery	Aspect Ratio	Dip	Mobility Ratio	Buoyancy Nb.	Capillary Nb.	Sgr	VDP
6	0,43	1,58	3,52	1,45	13,89	0,000301	0,38	0,6
10	0,1	6,32	0,17	1,45	1562,1	4,68	0,36	0,8

Figure 25. Dimensionless numbers corresponding to the minimum and maximum CO2 recoveries

As seen, the Aspect Ratio, Dip, Ng, Ca and VDP are extremes of the data base considered. Mobility and Sgr on the other hand are quite equal. It is clear that the higher value of the Ng favors the vertical segregation of the CO_2, causing a situation highly unfavorable to the recovery of the CO_2. Furthermore the high Aspect Ratio in which the vertical permeability is included only reinforces this situation.

5. CONCLUSIONS

- A representative Data-Base of potential storage candidates (aquifers) in terms of dimensionless groups governing the storage has been built from literature data. Yet, statistical evidence is still lacking, since many parameters needed to be borrowed from oil industry literature.
- A reduced experimental design (2k design) simplified has been used to study through simulations the CO_2 recovery, using a design in which the overpressure created by the injection is eased through the production of fluids.
- Recovery factors for CO_2 oscillate between 0.1- 0.43 for Injection Scenario 1 and 0.25 - 0.56 for Injection Scenario 2.
- Vertical movement due to parameters governing Aspect Ratio and Buoyancy (Ng), including Heterogeneity (VDP) and trapping characteristics are the most important aspects governing the setting of the CO_2 within a storage.
- Inasmuch as the reservoir pressure is re-established the production of the CO_2 can be considered as viable using two different strategies:
  - Either the CO_2 is left behind if the cap-rock is risk-free. In that case one can do without a high CO_2 recovery factor. Water storage becomes the main issue if reproduced.
  - Either the cap-rock being a risk in itself, it becomes worth producing most of the CO_2.

REFERENCES

[1] Shook, M. Lake, L.M. and Li, D.: "Scaling Immiscible Flow Through Permeable Media by Inspectional Analysis" In Situ, 16(4), 311-349, 1992

[2] Rivas, O., Embid, S. and Bolivar, F.: "Ranking Reservoirs for CO2 Flooding Processes", SPE 23641 presented at the 1992 SPE Latin American Petroleum Engineering Conference, Caracas, March 8-11

[3] Diaz, D., Bassiouni, Z., Kimbrell, W., and Wolcott, J. : "Screening Criteria for Application of Carbon Dioxide Miscible Displacement in Waterflooded Reservoirs Containing Light Oil", SPE 35431 presented at the 1996 SPE Improved Oil recovery Symposium, Tulsa, April 21-24

[4] Hirasaki, G., Steward W.C., Elkins, L.E., Wilhite, P.G. "Reply to Discussion of the National Petroleum Council Study on EOR", SPE 20007, Journal of Petroleum Technology, Nov. 1989

[5] Jensen JL, Lake LW, Corbett P, Goggin D. Statistics for petroleum engineers and geoscientists: Handbook of petroleum exploration and production 2 (HPEP). Elsevier, 2000.

[6] Dykstra, H, and R,L, Parsons: "The Prediction of Oil Recovery by Water Flood," Secondary Recovery of Oil in the United States, Principles and Practice, 2nd ed, Amer, Pet. Inst, (1950), 160-17 4.

[7] Bachu, S., Nordbotten, J.M., Celia, M.A. "Evaluation of the spread of acid gas plumes injected in deep saline aquifers in western Canada as an analogue for CO2 injection in continental sedimentary basins" GHGT-7 Paper ID Nb.12 revised

[8] Bachu, S., 2013. Drainage and imbibition CO2/brine relative permeability curves at in situ conditions for sandstone formations in Western Canada. Energy Proc. – 11th Int. Conf. Greenhouse. Gas Control Technol. 37, 4428–4436.

[9] Flett, M., Taggart, I., Lewis J., and Gurdon, R. "Subsurface sensitivity Study of Geologic CO2 Sequestration in Saline Formations" 2nd Annual Conf. on Carbon Sequestration, Alexandria, VA May 5-8, 2003.

[10] Hosa, A., Esentia, M., Stewart, J., Haszeldine S., "Benchmarking worldwide CO2 saline aquifer injections" Scottish Center for Carbon Capture and Storage, March 2010

[11] Salathiel, R., 1973. Oil recovery by surface film drainage in mixed-wettability rocks. J. Petrol. Technol. 25, 1216–1224.

[12] Taber, J., 1969. Dynamic and static forces required to remove a discontinuous oil phase from porous media containing both oil and water. SPE J. 9, 3–12.

[13] Lake, L., Johns, R., Rossen, B., Pope, G., 2014. Fundamentals of Enhanced Oil Recovery. Society of Petroleum Engineers, TX, USA.

[14] Broseta, D., Tonnet, N., Shah, V., 2012. Are rocks still water-wet in the presence of dense CO2 or H2S? Geofluids 12, 280–294.

[15] Chiquet, P., Broseta, D., Thibeau, S., 2007. Wettability alteration of cap-rock minerals by carbon dioxide. Geofluids 7, 112–122

[16] Iglauer, S., Pentland, C., Bush, A., 2014a. CO2 wettability of seal and reservoir rocks and the implications for carbon geosequestration. Water Resour. Res.
[17] Espinoza, D.N., Santamarina, J.C., 2010. Water-CO2-mineral systems: Interfacial tension, contact angle, and diffusion–implications to CO2 geological storage. Water Resour. Res. 46, W07537
[18] Farokhpoor, R., Bjorkvik, B., Lindeberg, E., Torsaeter, O., 2013. Wettability behavior of CO2 at storage conditions. Int. J. Greenh. Gas Control 12, 18–25.
[19] Wang, F., 1988. Effect of wettability alteration on water/oil relative permeability, dispersion, and flowable saturation in porous media. SPE Reserv. Eng. 3, 617–628.
[20] Saraji, S., Goual, L., Piri, M., Plancher, H., 2013. Wettability of supercritical carbon dioxide/water/quartz systems: Simultaneous measurement of contact angle and interfacial tension at reservoir conditions. Langmuir 29, 6856–6866.
[21] Iglauer, S., Salamah, A., Sarmadivaleh, M., Liu, K., Phan, C., 2014b. Contamination of silica surfaces: Impact on water-CO2-quartz and glass contact angle measurements. Int. J. Greenh. Gas Control 22, 325–328.
[22] Holtz, M.H., "Residual Gas Saturation to Aquifer Influx: A Calculation Method for 3-D Computer Reservoir Model Construction", SPE 75502, SPE Gas Technology Symposium held in Calgary, Alberta, Canada, 30 April–2 May 2002.
[23] Hadlow, R.E. "Update of Industry Experience with CO2 Injection" SPE 24928, 67th ATCE held in Washington, DC, October 4-7, 1992